force microscopy, and x-ray diffraction showed them to be atomically smooth over an area of 1 μm^2. The films were made superconducting by postannealing in ozone at 150 to 200°C for 10 to 30 min and quenching rapidly to room temperature to trap oxygen.
12. C. T. Chen *et al.*, *Phys. Rev. Lett.* **66**, 104 (1991).
13. C. T. Chen *et al.*, *Phys. Rev. Lett.* **68**, 2543 (1992).
14. F. C. Zhang, T. M. Rice, *Phys. Rev. B* **37**, R3759 (1988).
15. H. Eskes, M. B. J. Meinders, G. A. Sawatzky, *Phys. Rev. Lett.* **67**, 1035 (1991).
16. J. D. Jackson, *Classical Electrodynamics* (Wiley, New York, ed. 3, 1999).
17. Here $k = 2\pi/\lambda$, where λ is the x-ray wavelength and $n(\omega)$ is the refractive index.
18. We gratefully acknowledge the assistance of S. Hulbert, G. Nintzel, C.-C. Kao, and D. L. Feng and discussions with L. H. Tjeng, I. Elfimov, J. M. Tranquada, and J. C. Davis. Supported by an NSF IRFAP postdoctoral fellowship (INT0002581) and by the NWO (Dutch Science Foundation) via the Spinoza program. Work at the National Synchrotron Light Source is supported by the U.S. Department of Energy under contract no. DE-AC02-98CH109886.

14 February 2002; accepted 28 May 2002

Sliding Density Wave in $Sr_{14}Cu_{24}O_{41}$ Ladder Compounds

G. Blumberg,[1]* P. Littlewood,[1,2] A. Gozar,[1] B. S. Dennis,[1] N. Motoyama,[3] H. Eisaki,[4] S. Uchida[3]

We used transport and Raman scattering measurements to identify the insulating state of self-doped spin ½ two-leg ladders of $Sr_{14}Cu_{24}O_{41}$ as a weakly pinned, sliding density wave with nonlinear conductivity and a giant dielectric response that persists to remarkably high temperatures.

Investigation of the charge and spin dynamics of spin ½ low-dimensional transition metal oxide materials is attracting attention because of the critical nature of their ground state and the relevance to the phase diagram of high-temperature superconducting cuprates (*1, 2*). The competition between insulating states at low hole concentrations and superconductive pairing at higher hole densities has emerged as a key feature of the high-T_c (critical temperature) problem, but the character of the insulating states has remained elusive. Electronically one-dimensional (1D) materials are susceptible to a drastic change of their ground state to an insulator with spontaneous broken symmetry. For example, Peierls ordered states in which the links connecting nearest neighbor sites acquire modulated values for their charge and/or spin densities as well as for the exchange coupling constants are associated with broken translational symmetries and have been extensively discussed in the literature (*3*). In the charge-ordered state, collective excitations—such as those seen previously in sliding charge- and spin-density wave (C/SDW) compounds—should dominate the low-energy dynamics.

$Sr_{14}Cu_{24}O_{41}$ is an experimental realization of a two-leg ladder structure (Fig. 1). The planes of the weakly coupled Cu_2O_3 ladders are stacked along the crystallographic *b* axis alternating with 1D CuO_2 edge-sharing chain sheets (*4, 5*). The Cu-Cu distances in these two subunits are incommensurate but satisfy an approximate relation $10c_{chain} \approx 7c_{ladder}$. The legs and rungs of the ladders are along the *c* and *a* axes, respectively. Because the average valence of Cu is +2.25, the compound is intrinsically doped with holes believed to reside mainly in the chain substructure; optical studies have estimated 0.07 holes per ladder Cu site (*6*).

The self-doped compound $Sr_{14}Cu_{24}O_{41}$ is an insulator with an Arrhenius temperature dependence of the dc resistivity (*7*). Microwave (*8*) and magnetic resonance (*9*) studies have suggested the possibility of a charge ordering in the ladder planes that leads to insulating behavior. For ladders with higher hole concentrations, *d*-wave–like superconductivity was predicted to win the competition with the charge-ordered state (*1, 10*). Superconductivity at 12 K was discovered in doped two-leg ladders by applying both external and chemical pressure (*11*).

Single crystals of $Sr_{14}Cu_{24}O_{41}$ were grown as described in (*6, 12*). We have studied the low-frequency charge response by ac transport and Raman scattering experiments. The temperature dependence of the *c*-axis complex dielectric function between 10 and 10^6 Hz (Fig. 2A) was measured with a capacitive technique. The dc conductivity was measured by an electrometer (Fig. 3). Raman measurements (Fig. 2B) were performed from the (010) surface of the crystal as described in (*13*). We also report strong nonlinearity in the *c*-axis conductivity as a function of electric field.

The temperature dependence of the low-frequency Raman response function (Fig. 2B)

[1]Bell Laboratories, Lucent Technologies, Murray Hill, NJ 07974, USA. [2]University of Cambridge, Cavendish Laboratory, Cambridge CB3 0HE, UK. [3]University of Tokyo, Bunkyo-ku, Tokyo 113, Japan. [4]Stanford University, Stanford, CA 94305, USA.

*To whom correspondence should be addressed. E-mail: girsh@bell-labs.com

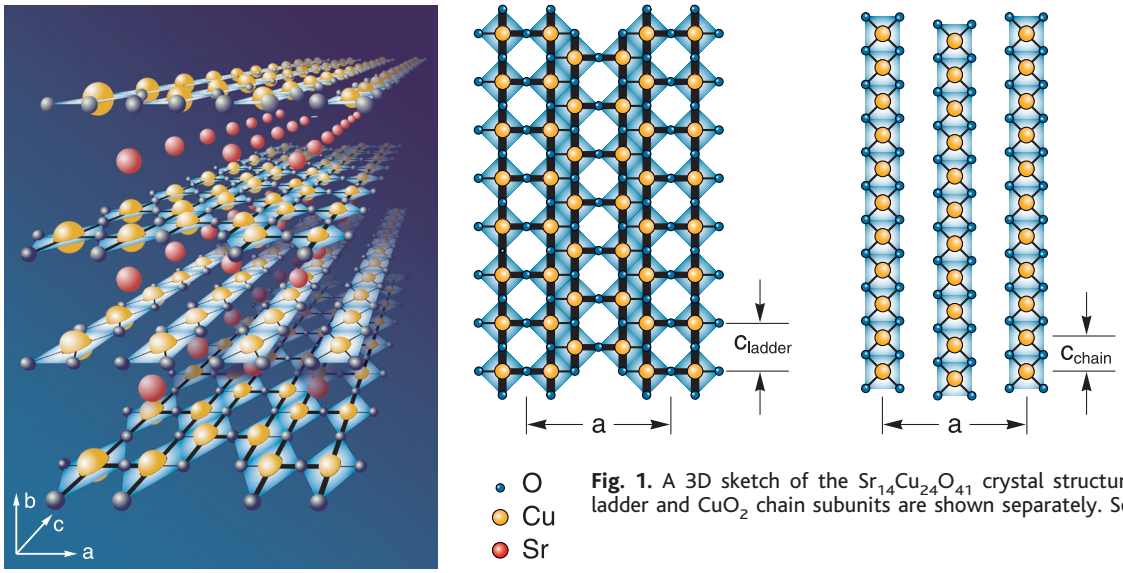

Fig. 1. A 3D sketch of the $Sr_{14}Cu_{24}O_{41}$ crystal structure. Three neighboring Cu_2O_3 ladder and CuO_2 chain subunits are shown separately. See (*4, 5*) for details.

shows a broad overdamped excitation below 1 meV (~250 GHz). This quasi-elastic scattering peak (QEP) rapidly shifts to lower frequencies with cooling. The data are fit by a relaxational form of the frequency (ω) dependent Raman response function

$$\chi''(\omega,T) = A(T)\,\frac{\omega\Gamma(T)}{\omega^2 + \Gamma(T)^2} \qquad (1)$$

The fit reveals a decrease in the QEP intensity, $A(T)$, with heating and an Arrhenius temperature dependence for the scattering rate $\Gamma(T)$ with an activation gap $\Delta \approx 2072$ K. The dc conductivity exhibits activated behavior with a break in the activation energy around $T^* \approx 150$ K: $\Delta \approx 1345$ K for $T < T^*$ and $\Delta = 2078$ K above T^*, similar to the activation energy observed for the Raman response function scattering rate $\Gamma(T)$ (Fig. 3). Similar quasi-elastic excitation has also been observed at high temperatures for superconducting Ca-doped $Sr_{14-x}Ca_xCu_{24}O_{41}$ ($0 < x < 12$) compounds with a higher concentration of holes in the ladder plane (*13*).

The frequency dependence of complex dielectric constant $\varepsilon = \varepsilon_1 + i\varepsilon_2$ is shown in Fig. 2A for temperatures between 85 and 150 K. The low-frequency response of ε_2 shows overdamped, inhomogeneously broadened peaks at characteristic frequencies $\nu_0(T)$ determined by damping parameters $\Gamma(T) = 2\pi\nu_0(T) = \tau^{-1}$ [where $\tau(T)$ is the relaxation time]. Strong relaxational peaks lead to a giant real part of the dielectric response ε_1 below $\nu_0(T)$ observed up to room temperature and even above. Such behavior is incompatible with any single-particle theory, as it would imply energy gaps more than six orders of magnitude smaller than the thermal energy and suggests that the low-frequency charge dynamics is driven by correlated collective behavior.

In Fig. 4 we scale all the measured complex dielectric functions between 80 and 160 K on one universal generalized Debye relaxational curve,

$$\varepsilon(\omega) = \varepsilon_\infty + \frac{\varepsilon_0 - \varepsilon_\infty}{1 + [i\omega\tau(T)]^{1-\alpha}} \qquad (2)$$

where ε_0 and ε_∞ are low- and high-frequency dielectric constants and the fitted value $\alpha = 0.42$ characterizes the width of the distribution of relaxational times (*14*). The temperature dependences of the scattering rates $\Gamma(T) = \tau^{-1}$ from ac transport and Raman measurements are compared to the dc conductivity in Fig. 3: The scattering rates $\Gamma(T)$ follow the activated behavior of dc conductivity over 10 decades of frequency.

We now discuss the implications of these observations. First, we note that recent microwave experiments by Kitano *et al.* have reported a relatively small and narrow peak between 30 and 100 GHz in the *c*-axis conductivity observed up to moderately high temperatures (*8*). This resonance is attributed by the authors to a collective excitation of a pinned charge-density wave (CDW).

In the charge or spin density state, the condensed electrons do not participate in the conduction process for small dc electric fields. The reason for this is the interaction between the condensate and impurities and other lattice irregularities. This pinning shifts the oscillator strength associated with the collective modes to finite frequencies, with no contribution to the dc conductivity that shows an activated behavior, and is entirely determined by quasiparticle excitations out of the condensate. The Arrhenius law for the decay constant $\Gamma(T)$ suggests a hydrodynamic origin for the Raman and low-frequency conductivity modes, for which there is considerable precedent in studies of the dynamics of pinned CDW and SDW systems (*15–20*), and we compare the $Sr_{14}Cu_{24}O_{41}$ ladder system to well-established models of CDW dynamics (*21*). The pinned collective mode can be described by an oscillator making a collective contribution to the ac conductivity

$$\sigma_{coll}(\omega) = \frac{1}{4\pi}\,\frac{-i\omega\Omega_p^2}{\Omega_0^2 - \omega^2 - i\gamma_0\omega} \qquad (3)$$

where $\Omega_p^2 = \rho_c^2/m^*$ is the oscillator strength of the mode with charge density ρ_c and mass density m^*, Ω_0 is the pinning frequency, and γ_0 is an intrinsic damping coefficient. To account for the longitudinal response (relevant for Raman scattering), we must allow for screening of the collective mode. Then the longitudinal response function is

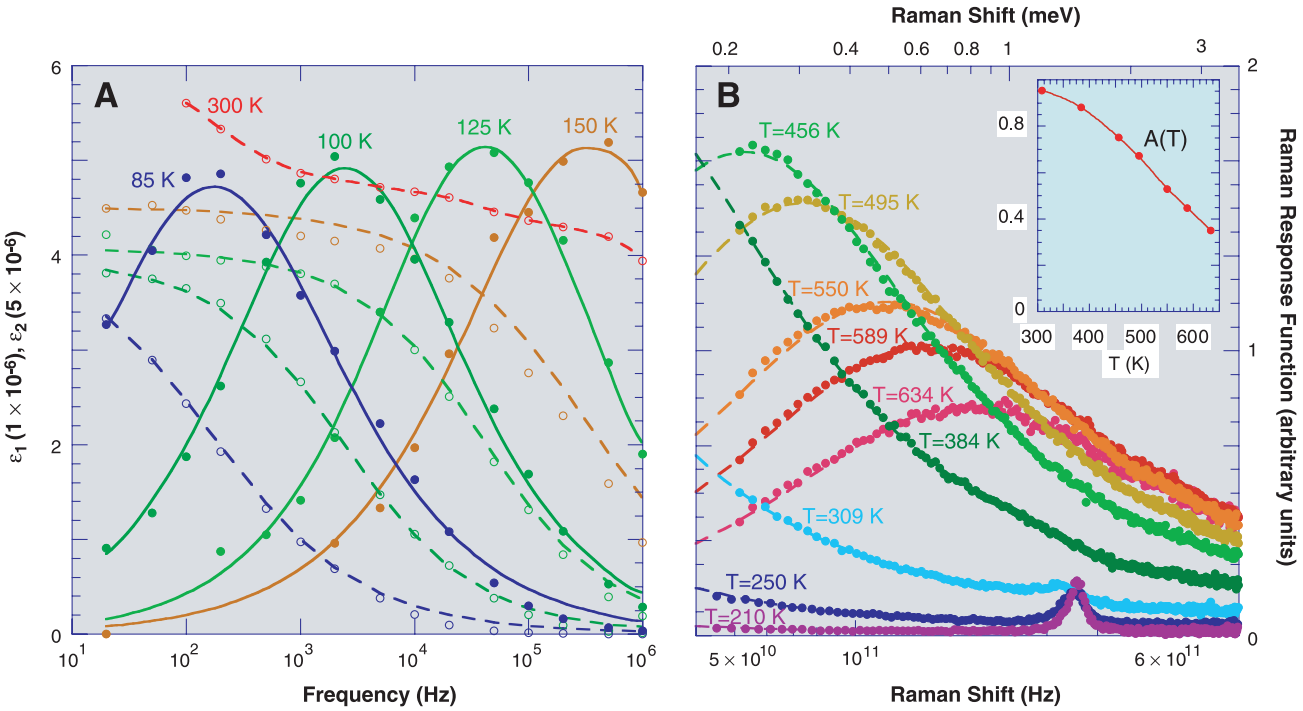

Fig. 2. (**A**) The temperature dependence of the measured real (open circles) and imaginary (solid circles) parts of the complex dielectric function between 85 and 300 K. The dashed and solid lines are guides for the eye. (**B**) The temperature dependence of the Raman response function for the polarization of the incident and scattered photons parallel to the legs of the ladders: the data (circles) and the fit to Eq. 1 (dashed lines). The spectra were acquired in a backscattering geometry using the 7993 Å excitation. The resonance at about 356 GHz at low temperatures is a phonon. The inset shows the diminishing quasi-elastic scattering intensity, $A(T)$, with heating.

$$\varepsilon_L(\omega) = \frac{\Omega_p^2}{\Omega_0^2 - \omega^2 - i\gamma_0\omega - \left(\frac{i\omega\Omega_p^2}{4\pi\sigma_{qp} - i\omega\varepsilon_\infty}\right)} \quad (4)$$

where σ_{qp} is the dc "background" conductivity due to quasi-particle transport. Note that at low frequency, Eq. 4 reduces to a relaxational mode, with amplitude Ω_p^2/Ω_0^2 and decay constant

$$\Gamma(T) = 4\pi\sigma_{qp}\frac{\Omega_0^2}{\Omega_p^2} = \frac{4\pi\sigma_{qp}}{\varepsilon_0 - \varepsilon_\infty} \quad (5)$$

The proportionality of $\Gamma(T)$ and σ_{qp} arises because the collective charge oscillations are screened by thermally excited and uncondensed quasi-particle carriers on the relevant ladder. Although the longitudinal mode we are discussing is in principle neutral, the effects of disorder in a strongly anisotropic system make it visible—in fact typically dominant—in the transverse response, and therefore it will contribute to ac conductivity. Such was the case in CDW systems (*15–20*). The transfer of spectral weight to the longitudinal channel explains why the oscillator strength in the microwave region (*8*) is anomalously small.

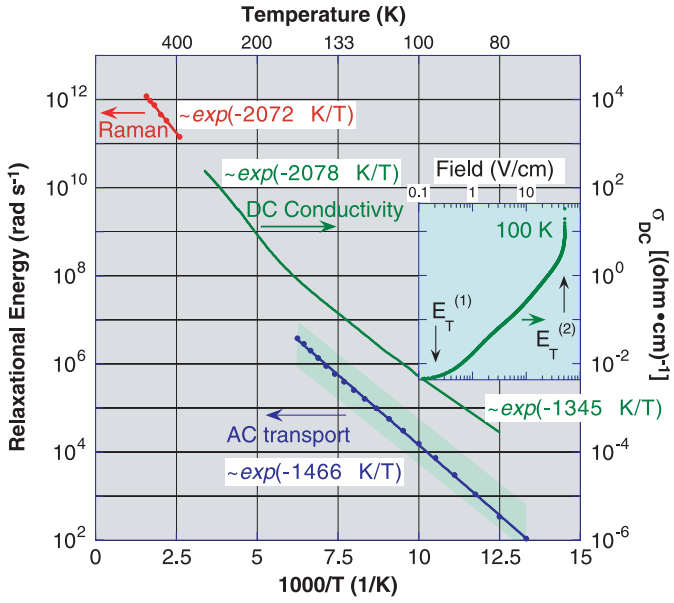

Fig. 3. The temperature dependence of the scattering rates (left scale) $\Gamma(T) = \tau^{-1}$ from scaling of the ac dielectric (Fig. 4) and Raman (Fig. 2B) response. The scattering rate follows the activated behavior of the dc conductivity (right scale) over 10 decades of frequencies. The inset shows strong nonlinearity in the dc conductivity as a function of electric field measured at 100 K.

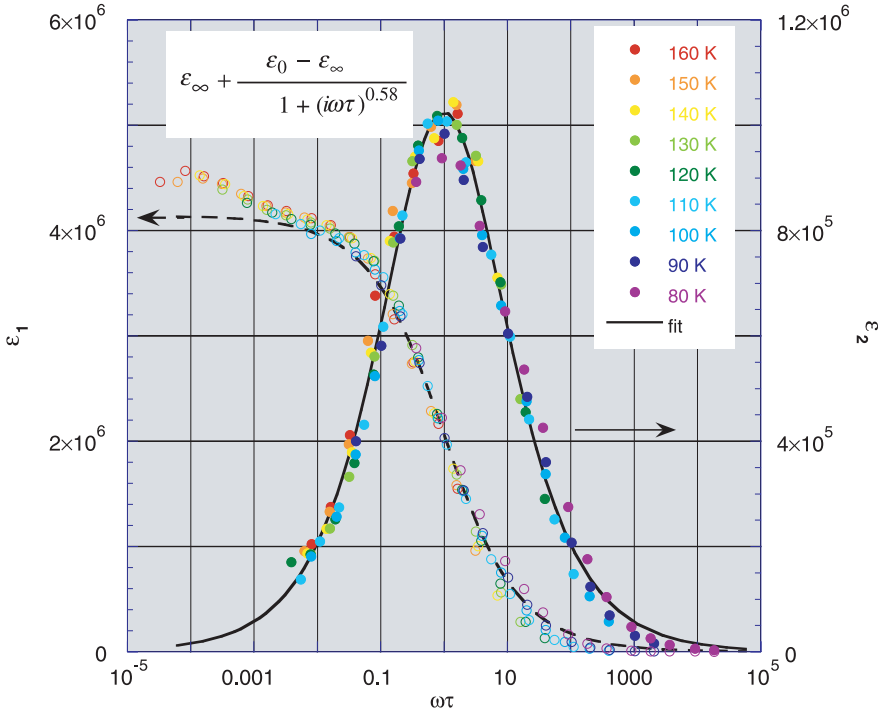

Fig. 4. Scaling, measured between 80 and 160 K in the 20 Hz to 1 MHz frequency window, of the complex dielectric function (imaginary part, solid circles; real part, open circles) on the generalized Debye relaxational curve (*2*). The obtained temperature-dependent scattering rate $\Gamma(T) = \tau^{-1}$ is shown in Fig. 3.

The plasma edge energy for $Sr_{14}Cu_{24}O_{41}$, determined from IR spectroscopy as the peak position of the loss function $\Im[-1/\varepsilon(\omega)]$, gives us an estimate for $\Omega_p \approx 3300\ cm^{-1}$ (*6, 22*). Using the characteristic pinning frequency $\Omega_0 \approx 30$ to 100 GHz suggested by microwave measurements (*8*), we estimate the value of the low-frequency dielectric constant $\varepsilon_0 \approx \Omega_p^2/\Omega_0^2$ to be between 10^6 and 10^7, which is consistent with our direct measurements. Following Eq. 5 and the estimated values for ε_0, we calculate the theoretical values for $\Gamma(T)$ using the measured dc conductivity. These calculated values are shown by the shaded green area in Fig. 3. They are in very good agreement with the relaxational energies extracted from the peaks in $\varepsilon_2(\omega)$ (see Fig. 4). The overall consistency among the measured temperature dependences of the dielectric response $\varepsilon(\omega)$, the relaxation rate $\Gamma(T)$, and the dc conductivity σ_{qp} demonstrates the applicability of the hydrodynamic model description for the low-frequency collective charge dynamics in this system. Moreover, the broad inhomogeneous response has exactly the character expected for random pinning by disorder of an incommensurate density wave.

The low-frequency Ω_0, which describes the oscillation of the collective mode about the pinned equilibrium position, implies a weak restoring force. Therefore, it is anticipated that a small dc electric field can induce sliding density wave transport by translational motion of the condensate. In the inset of Fig. 3 we show conductivity at 100 K measured as a function of applied electric field. Below a threshold field $E_T^{(1)} \approx 0.2$ V/cm, the conductivity obeys Ohm's law with the Arrhenius temperature dependence discussed above. However, for electric fields above the $E_T^{(1)}$ threshold, the *I-V* characteristics change from linear to approximately quadratic, indicating an onset for sliding density wave conductivity (*23*). In this regime of relatively slow CDW sliding, the predominant damping mechanism is the screening of internal electric fields produced by local CDW deformations by backflow currents of uncondensed quasi-particles (*21*).

At much higher fields, above 50 V/cm, we observe a second threshold, $E_T^{(2)}$, with a very sharp rise of the current up to the limit of the current generator. The calculated differential conductivity in this regime is enormous,

more than $10^5\ \Omega^{-1}\ cm^{-1}$, an estimate limited by contact effects and most likely carried by inhomogeneous filamentary conduction. We attribute this phenomenon to the crossover to a regime of free sliding CDW first proposed by Fröhlich as CDW superconductivity (*24*). Such a crossover has been observed in conventional CDWs, and is expected to occur once the density wave reaches velocities at which the background quasi-particles can no longer screen the response (*25*). An upper limit of the field at this second threshold may be estimated from the average pinning frequency $E_T^{(2)} \leq (\Omega_0^2/\Omega_p^2)(\rho_c/Q)$, where ρ_c is the collective charge density and $2\pi/Q$ is the period of the density wave. Assuming $2e$ per ladder (where e is electronic charge) contributing to the density wave, we obtain $E_T^{(2)} \leq$ 100 V/cm, again consistent with our measurements. Note that the true threshold for deformable sliding of the density wave is always much lower.

Now we turn to high-temperature Raman measurements. The Raman response function is proportional to $\Im\varepsilon_L$. The comparison of the Raman and ac transport data is not straightforward because only above room temperature is $\Gamma(T)$ large enough for a Raman QEP to be observed. Although $\Gamma(T)$ extracted from the Raman data exhibits activated behavior with a gap consistent with dc conductivity above T^*, the values for $\Gamma(T)$ are about 50 times the relaxational energies predicted from Eq. 5. However, the lowering of the peak intensity with increasing temperature (see Fig. 2B, inset) suggests that there is a reduction of the density wave amplitude ρ_c, which would produce a concomitant increase in Γ. Further enhancement in the scattering rate may come from additional relaxation due to the presence of low-lying states seen at temperatures above T^* by magnetic resonance (*9*), high-frequency Raman scattering (*26*), and *c*-axis optical conductivity (*22*).

All our results have clear quantitative parallels with sliding density wave transport phenomena observed in established C/SDW materials, yet there must be a number of important microscopic differences from conventional weak-amplitude C/SDWs. The C/SDW correlation in $Sr_{14}Cu_{24}O_{41}$ is a high-temperature phenomenon that we observe (with diminishing amplitude) up to the highest measured temperature, 630 K. Such high-temperature correlations cannot be supported by phonons, which suggests that the charge-spin correlations arise from strong spin exchange interactions with characteristic energy scale $J \approx 1300$ K (*26*). The magnetic excitations in spin ½ two-leg ladders are resonating valence bond (RVB) quantum states (*1, 3, 26, 27*), different from the gapless classical spin waves in the SDW systems. Theoretical calculations for a doped two-leg spin ladder suggest that in an RVB environment the holes are paired in a state of approximate *d*-wave symmetry with a few lattice spacings in size (*28–30*). The superconducting condensation of bound pairs is competing with a crystalline order of these pairs in a CDW state (*10*). If the fundamental current-carrying object in the doped singlet ladders is a bound pair of holes, the hydrodynamic mode we have discussed involves local displacement of "crystallized" pairs, screened by charged excitations across the CDW gap, which would account for the appearance of the conductivity as the relevant parameter to describe backflow. Nevertheless, our observation of a weakly pinned mode—which implies a large stiffness for charged fluctuations of the order parameter—is surprising in the context of models with strong short-range correlations, where one would expect that lattice pinning effects are strong.

References and Notes

1. E. Dagotto, T. M. Rice, *Science* **271**, 618 (1996).
2. E. Dagotto, *Rep. Prog. Phys.* **62**, 1525 (1999) and references therein.
3. S. Sachdev, *Science* **288**, 475 (2000) and references therein.
4. E. M. McCarron III, M. A. Subramanian, J. C. Calabrese, R. L. Harlow, *Mater. Res. Bull.* **23**, 1355 (1988).
5. T. Siegrist, L. F. Schneemeyer, S. A. Sunshine, J. V. Waszczak, R. S. Roth, *Mater. Res. Bull.* **23**, 1429 (1988).
6. T. Osafune, N. Motoyama, H. Eisaki, S. Uchida, *Phys. Rev. Lett.* **78**, 1980 (1997).
7. M. W. McElfresh, J. M. D. Coey, P. Strobel, S. von Molnar, *Phys. Rev. B* **40**, 825 (1989).
8. H. Kitano *et al.*, *Europhys. Lett.* **56**, 434 (2001).
9. M. Takigawa, N. Motoyama, H. Eisaki, S. Uchida, *Phys. Rev. B* **57**, 1124 (1998).
10. E. Dagotto, J. Riera, D. J. Scalapino, *Phys. Rev. B* **45**, 5744 (1992).
11. M. Uehara *et al.*, *J. Phys. Soc. Jpn.* **65**, 2764 (1996).
12. N. Motoyama, T. Osafune, T. Kakeshita, H. Eisaki, S. Uchida, *Phys. Rev. B* **55**, R3386 (1997).
13. A. Gozar *et al.*, http://arXiv.org/abs/cond-mat/0207219 (2002).
14. S. Havriliak, S. Negami, *J. Polym. Sci. C* **14**, 99 (1966).
15. G. Grüner, L. C. Tippie, J. Sanny, W. G. Clark, N. P. Ong, *Phys. Rev. Lett.* **45**, 935 (1980).
16. W.-Y. Wu, L. Mihály, G. Mozurkewich, G. Grüner, *Phys. Rev. Lett.* **52**, 2382 (1984).
17. R. J. Cava *et al.*, *Phys. Rev. B* **30**, 3228 (1984).
18. R. J. Cava, P. Littlewood, R. M. Fleming, R. G. Dunn, E. A. Rietman, *Phys. Rev. B* **33**, 2439 (1986).
19. L. Degiorgi, B. Alavi, G. Mihály, G. Grüner, *Phys. Rev. B* **44**, 7808 (1991).
20. G. Grüner, *Density Waves in Solids* (Perseus, Cambridge, MA, 1994).
21. P. B. Littlewood, *Phys. Rev. B* **36**, 3108 (1987).
22. H. Eisaki *et al.*, *Physica C* **341–348**, 363 (2000).
23. A. Zettl, G. Grüner, A. H. Thompson, *Phys. Rev. B* **26**, 5760 (1982).
24. H. Fröhlich, *Proc. R. Soc. London Ser. A* **223**, 296 (1954).
25. P. B. Littlewood, *Solid State Commun.* **65**, 1347 (1988).
26. A. Gozar *et al.*, *Phys. Rev. Lett.* **87**, 197202 (2001).
27. P. W. Anderson, *Science* **235**, 1196 (1987).
28. M. Sigrist, T. M. Rice, F. C. Zhang, *Phys. Rev. B* **49**, 12058 (1994).
29. M. Troyer, H. Tsunetsugu, T. M. Rice, *Phys. Rev. B* **53**, 251 (1996).
30. S. R. White, D. J. Scalapino, *Phys. Rev. B* **55**, 6504 (1997).

31. We thank A. P. Ramirez for help with ac transport measurements and for discussions. Supported by a Grant-in-Aid for Scientific Research and a COE grant from the Ministry of Education, Japan (S.U.).

1 February 2002; accepted 31 May 2002

Delocalization of Protons in Liquid Water

H. J. Bakker* and H.-K. Nienhuys†

We find that the vibrational potential of the O-H stretch vibrations of liquid water shows extreme anharmonicity that arises from the O-H · · · O hydrogen bond interaction. We observe that already in the second excited state of the O-H stretch vibration, the hydrogen atom becomes delocalized between the oxygen atoms of two neighboring water molecules. The energy required for this delocalization is unexpectedly low and corresponds to less than 20% of the dissociation energy of the O-H bond of the water molecule in the gas phase.

Liquid water possesses many remarkable properties that to a large extent can be explained by its extremely high density of hydrogen bonds. One of these properties is the anomalously high mobility of protons and hydroxyl ions (OH^-) in this liquid. This phenomenon has been explained from a (Grotthuss) conduction mechanism (*1*) that involves the exchange of the chemical O-H bond and the hydrogen bond in the O-H · · · O hydrogen-bonded system formed by an H_3O^+/OH^- ion and an H_2O molecule (*2–4*).

Relatively little is known about the effects of hydrogen bond interactions in liquid water on the reactivity of the O-H groups of the water molecule. In most molecular dynamics simulations, these effects are not included. Even in the most advanced Car-Parrinello molecular dynamics simulations, these effects are not well accounted for because the nuclear coordinates are described classically. In view of the small mass of the hydrogen atom and the proton, such a classic approach gives a poor description of the properties of

FOM Institute for Atomic and Molecular Physics, Kruislaan 407, 1098 SJ Amsterdam, Netherlands.

*To whom correspondence should be addressed. E-mail: bakker@amolf.nl

†Present address: Department of Chemical Physics, Lund University, Box 124, 221 00 Lund, Sweden.